



A NEW ROBOTIC SYSTEM FOR MINIMALLY INVASIVE TREATMENT OF LIVER TUMOURS

Calin VAIDA¹, Nicolae PLITEA¹, Nadim AL HAJJAR², Alin BURZ¹, Florin GRAUR², Bogdan GHERMAN¹, Doina PISLA¹

¹ Research Center for Industrial Robots Simulation and Testing, Technical University of Cluj-Napoca, Romania

² “Iuliu Hatieganu” University of Medicine and Pharmacy, Cluj-Napoca, Romania

Corresponding author: Doina PISLA, E-mail: Doina.Pisla@mep.utcluj.ro

Abstract. The non-surgical treatment of hepato-cellular liver carcinoma is an open problem as no current approach seems to reduce its mortality. The authors propose a new medical approach using a robotic system that enables the targeted liver tumour therapy with real time ultrasound guidance during the procedure, performed as a minimally invasive procedure inside the operating room. A dual arm robotic system based on innovative parallel structures is developed to guide both the therapeutic needles inside the tumours and the intraoperative ultrasound probe which can monitor the needle insertion inside the tumours. The paper focuses on the kinematics of the ultrasound probe guiding module which performs complex motions inside the body and its validation with numerical simulations.

Key words: parallel robot, kinematics, numerical simulations, hepatocellular carcinoma.

1. INTRODUCTION

Hepatocellular carcinoma (HCC) is the most common primary liver tumour accounting for over 800,000 new cases annually being also the fourth leading cause of cancer-related death due to a very high mortality index (0.93) [1, 2]. While the most important risk for HCC is cirrhosis (80% to 90% of the patients), patients with HCC have most often other underlying diseases. Due to these reasons, the treatment of HCC is not straightforward and must be carefully chosen to provide an increase in the survival of the patients. Currently, worldwide there are two curative options for HCC [3]: orthotopic liver transplantation (OLT) and resection. While the transplantation is the best curative option there are very few available donors leaving only resection as a large scale therapy. Even though many centres have pushed the existing guidelines (in terms of maximum resection volume) only around 20% of the HCC patients qualify for surgery. For the remaining 80% there are local and systemic approaches which use other means to destroy or downgrade the tumours: TACE (transarterial chemoembolization), RFA (radiofrequency ablation), microwave and cryoablation, percutaneous ethanol injection, high-intensity focused ultrasound, external beam radiation, to name the most used ones [3, 4]. However due to a large number of variables (tumour location, adjacent blood vessels, co-morbidities, prior treatments) there is no specific therapy which provides better results [2].

Besides systemic or external treatments (which have multiple side effects) the local, targeted procedures are many times hindered because of the tumours location inside the liver parenchyma which imposes careful and highly accurate positioning of the treatment delivering tools. As the required accuracy is often higher than the human capabilities [5] a specialized device or a robotic arm should be used for the positioning task. The main constraint for the use of targeted therapies for the liver refers to the difficult patient-robot calibration, currently only RFA being used in open surgery.

This paper presents a parallel robotic system designed to treat HCC tumours using either HDR (High Dose Rate) brachytherapy or intratumoral drug delivery with real-time ultrasound monitoring. The novelty items refer to the overall treatment technique and the new robotic system developed to fulfill the medical requirements which is based on a patent pending [11]. The new system enables the accurate location of the tumour using the real-time data from the I-US that eliminates the pre-surgical patient-robot calibration. The

medical procedure is performed in a minimally invasive way using an intraoperative ultrasound probe to accurately locate and supervise the needle insertion procedure. As the two motions have to be synchronized, a dual-arm robotic system should be used.

The paper presents in section 2 a detailed description of the medical protocol which defines the main specifications of the robotic system. Section 3 analyses the specific motions for the intraoperative ultrasound probe guiding module and its kinematics. Section 4 presents numerical simulations of the robotic module while manipulating the probe outside and inside the human body.

2. MEDICAL APPLICATION

The IMPROVE vision [6] regarding the non-surgical treatment of HCC tumours has three main stages: (a) the preoperative procedure where multiple non-invasive image processing techniques are used to accurately locate and diagnose the targeted liver tumour(s) along with the selection of the optimum therapeutic approach based on the patient specific conditions; (b) the intraoperative stage where, in a minimally invasive approach, inside the operating room the robotic system performs a real-time ultrasound monitored placement of the catheters (needles) for the treatment delivery, followed by the actual application of the therapy; (c) post-operative patient monitoring for possible recurrence and adjuvant treatments. The paper focuses on the intraoperative stage of the procedure that is described as a medical protocol in Table 1.

Materials required for the procedure: (1) the procedure takes place in the operating room, which has all the necessary equipment in a setup presented in Fig. 1, where the robot and the computer processing unit have to be integrated; (2) the patient is positioned on the surgical bed which can be adjusted in terms of height and orientation along all three axes to provide suitable access to the area of the liver where the tumour(s) is located (Fig. 2); (3) three instruments are required: an intraoperative ultrasound (I-US) probe that is guided by one parallel robotic module, a therapeutic catheter that will be guided by the second module and a manually guided laparoscopic camera that is used to monitor the procedure inside the patient. Both instruments that are robotic guided are installed in dedicated modules which perform specific tasks.



Fig. 1 – Typical configuration of the operating room.

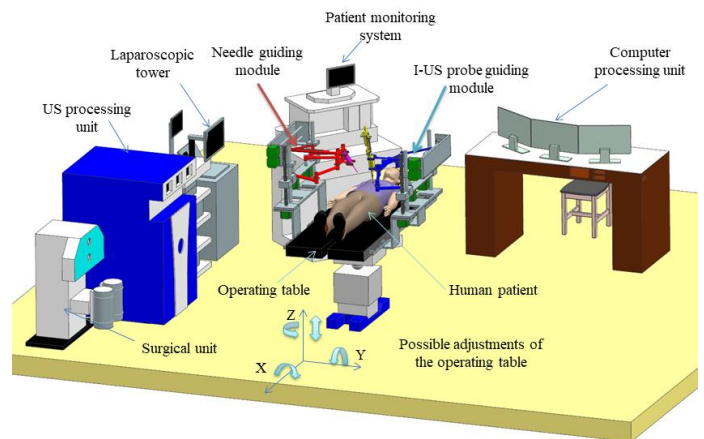


Fig. 2 – Virtual operating room with the robotic unit and possible operating table motions.

Table 1

A stepwise medical protocol for the intraoperative non-surgical treatment of HCC tumours

Step	Specific procedure
1.	The patient undergoes general anaesthesia and the abdominal area is inflated with carbon dioxide up to a pressure of 10 mmHg creating the necessary cavity for the instruments. The robotic arms are covered with a sterile plastic foil leaving outside just the end-effector connection element to the instruments.
2.	A trocar (device through which the instruments are introduced, which has a double role: to maintain the pressure inside the abdomen through an elastic membrane and to protect the abdomen wall when the instruments are manipulated) is introduced on the median line of the abdomen for the laparoscopic camera which will be handled during the procedure by an assistant.

Step	Specific procedure
3.	A second trocar is positioned in a suitable way to provide best access to the targeted area of the liver based on the pre-planning of the procedure.
4.	The I-US probe is attached to the first robot module and introduced through the second trocar, then guided towards the liver.
5.	Based on the preoperative data the probe is positioned on the liver parenchyma in the area of interest and then by accurate motions the tumour is accurately located. Having all the dimensional parameters of the I-US introduced in the kinematic model of the robotic arm, the coordinates of the target point inside the tumour and the insertion vector are recorded in the robot control system, being used as input for the second robotic arm (thus solving the calibration problem).
6.	The second robotic arm which holds the therapeutic needle(s) is calibrated with respect to the patient using several external body markers defined in the preoperative stage and registered also with respect to the first arm.
7.	Based on the preoperative data a set of points (I – insertion and T - target) are defined for the needle using the data from step 5. As the two robotic arms are registered one with respect to the other, the I-US probe is kept aligned to the defined needle trajectory inserted by the second arm. This will enable the real-time visualization of the needle as it is inserted in the liver.
8.	Using the robotic arm the needle is positioned with the tip in the insertion point and the final orientation defined by the I-T pair of points [7].
9.	The needle is driven through the skin and it is visualized inside the abdominal area using the laparoscopic camera. Once the liver parenchyma is reached the position is verified one more time and if necessary small corrections are applied. In case the needed corrections are larger, the needle will be retracted and inserted again.
10.	In case the procedure requires the insertion of multiple needles the next needle is loaded and the steps 7 to 9 are repeated for each new needle.
11.	Once all the needles are inserted, the IU-S probe is used to verify and validate the final needle(s) positions and the specific therapy is applied.
12.	When the therapy is finished the needles are extracted manually and using the laparoscopic camera the surgical field is inspected for any signs of bleeding. If necessary, haemostasis is applied.
13.	The IU-S probe is retracted, using the robotic arm, followed by the manual extraction of the laparoscopic camera and the procedure is finished.

2.1. ProHep-LCT – a new robotic system for the non-surgical treatment of HCC tumours

Based on the defined specifications, the robotic system should have the following characteristics:

- the robot should be fixed on the lateral sides of the operating table (see Fig. 2);
- the needle positioning module should have 5 DoF (the rotation around the longitudinal axis of the needle is not required [8]);
- the I-US probe guiding module should have 5 DoF;
- on the needle positioning module a special device with 1 DoF is needed to perform the insertion of the needle in a safe way while monitoring continuously the tissue resistance [8, 9]; an experimental analysis of the needle behaviour during the insertion in deformable tissues will be performed to pork liver using a calibrated press with a sensor mounted on the proximal needle head to monitor the tissue behaviour during the needle insertion, its resistance and friction; the medical needles used for the procedure have a diameter of 1.6 mm with a sharp cutting edge to minimize tissue deformation during insertion while the real-time monitoring of the needle position will ensure the accurate tumour targeting;



Fig. 3 – The I-US probe.

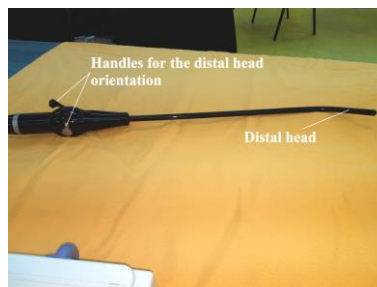


Fig. 4 – The handles used to bend the instrument head.

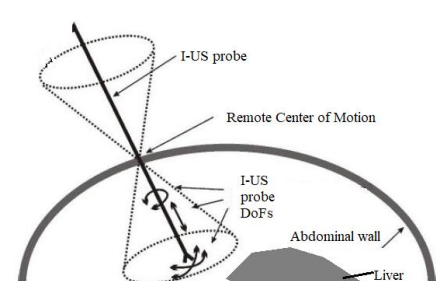


Fig. 5 – Schematic representation of the RCM and the 4 DoFs of the probe.

- the I-US probe (Fig. 3) has a distal head which can be oriented around two axes using the two handles located in the proximal end (Fig. 4); in addition the US transducer is located on one side of the distal

head which means that the I-US probe must be rotated around its longitudinal axis; these characteristics impose a total of 9 DoF for the I-US probe, 5 being achieved by the robot, namely three rotations and two translations [12] and an additional 4 DoF achieved by the end-effector: 2 DoF for the actuation of the handles for the orientation of the I-US distal head, one for the orientation of the transducer that has to be placed directly on the liver and one for the I-US translation along its longitudinal axis;

– the I-US probe has to perform complex motions inside the body (Fig. 5), based on the concept of the remote centre of motion (RCM) located at the entrance point inside the body [10].

We performed a literature survey which revealed that regarding robotic assisted intraoperative US only the da Vinci system has a proprietary instrument (BK5000) for this task and to our best knowledge there are no documented results regarding the entire procedure proposed by our team, which emphasizes its novelty.

A new robotic system, ProHep-LCT has been developed in order to achieve in an optimum way the motions defined at the level of each module, its complexity being imposed by the procedure [11]. The total number DoFs for each of the two robotic arms is five (5). The entire system is presented in Fig. 6, while a kinematic scheme of the probe guiding module is illustrated in Fig. 7.

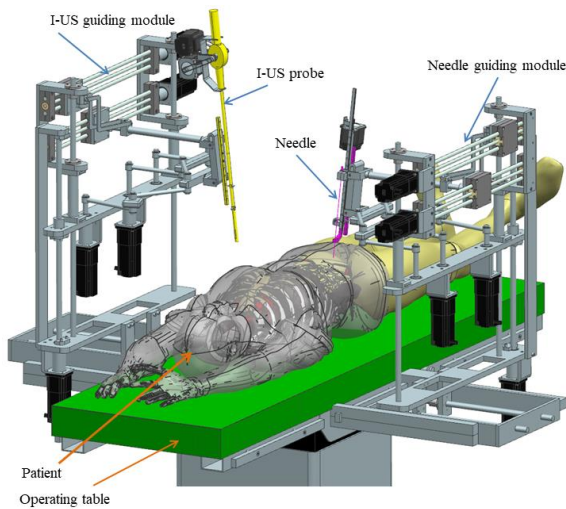


Fig. 6 – The ProHep-LCT robotic system.

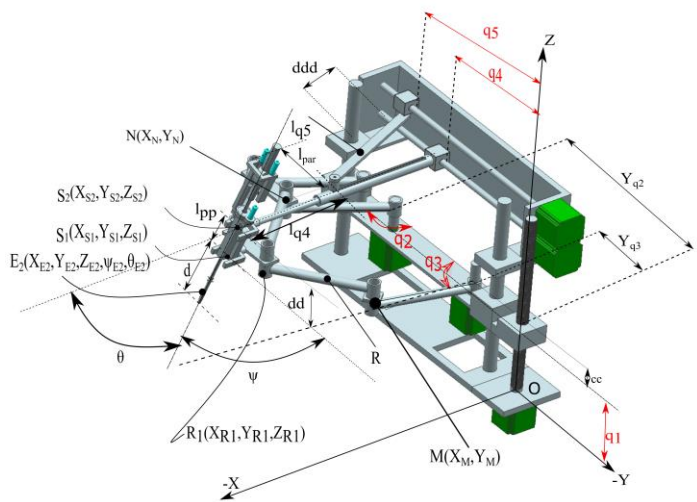


Fig. 7 – The kinematic scheme of the I-US guiding probe.

The two modules shown in Fig. 6 have similar kinematics: the base module is a 2-DoF parallel module with constant platform orientation actuated by the joints (q_2 and q_3 which rotate around the OZ axis) while the top module is a 2-DoF module working in cylindrical coordinates (actuated by the translational joints q_4 and q_5 along the OY axis), the two modules being connected through a pair of Cardan joints which rotate along the X and Y axes. The two modules are translated vertically by the joint q_1 while having a constant distance between them. A fixed coordinate system $OXYZ$ is attached to the robot base with the Z axis along the translation axis of the planar modules, the X and Y axes being defined with respect to the human body axes while a mobile one is attached to the I-US probe. The kinematic model of the needle positioning module has been presented in [12]. The I-US probe guiding module requires special attention as from the application point of view, with respect to the procedure step (Table 1) different kinematic models have to be used:

– when the I-US probe is located outside the body the mechanism will behave as a 5-DoF robot;

– when the I-US probe is located inside the body it will have to pass always through the insertion point (the RCM) which from kinematic point of view behaves as a class 2 joint, which restricts the number of DoF of the robot to only three (3).

3. KINEMATIC MODELLING OF THE I-US PROBE GUIDING MODULE

The following notations are introduced to solve the kinematic model (Fig. 7):

- R – the link length between two rotational joints of the lower planar parallel mechanism;
- l_{par} – the distance between the pairs of links forming the parallelogram of the lower mechanism;
- l_{q4} , l_{q5} – the lengths of the rods connecting the upper Cardan joint to the active joints q_4 and q_5 ;

- Y_{q_2}, Y_{q_3} – the distance on Y axis of the rotational axes of the active joints q_2 and q_3 ;
- l_{pp} – the distance along the Z axis between the two planar modules;
- S_1, S_2 – the intersection point of the rotational axes of the lower and respectively upper Cardan joints;
- d – the distance between the point S_1 and the probe tip;
- cc – the distance on the Z axis between S_1 and q_1 ;
- dd – the distance on X axis between and the mobile platform of the lower mechanism;
- ddd – the distance along the X axis between the OX axis and the axis of q_4 and q_5 .

Case 1. The I-US probe is located outside the body. The input parameters are: $X_{E2}, Y_{E2}, Z_{E2}, \psi_{E2}, \theta_{E2}$ which define the position of the I-US tip and its orientation with respect to the fixed coordinate system.

Based on the rotational axes of the Cardan joint, to avoid the parametrization singularity of the Euler angles, the YX convention was used. The coordinates of the first Cardan joint are:

$$\begin{cases} X_{S1} = X_{E2} - d \cdot \sin(\theta_{E2}) \\ Y_{S1} = Y_{E2} + d \cdot \cos(\theta_{E2}) \cdot \sin(\psi_{E2}) \\ Z_{S1} = Z_{E2} + d \cdot \cos(\theta_{E2}) \cdot \cos(\psi_{E2}) \end{cases} \quad (1)$$

As the vertical distance between the two planar modules is constant, the distance between S_1 and S_2 has to be computed and used to determine the coordinates of S_2 :

$$l_p = \frac{l_{pp}}{\cos(\theta_{E2}) \cdot \cos(\psi_{E2})}, \quad \begin{cases} X_{S1} = X_{E2} - (d + l_p) \cdot \sin(\theta_{E2}) \\ Y_{S1} = Y_{E2} + (d + l_p) \cdot \cos(\theta_{E2}) \cdot \sin(\psi_{E2}) \\ Z_{S1} = Z_{E2} + (d + l_p) \cdot \cos(\theta_{E2}) \cdot \cos(\psi_{E2}) \end{cases} \quad (2)$$

The coordinates of the active joints q_2 and q_3 are calculated using the properties of intersecting circles. Thus, the coordinates of point S_{23} are calculated, along with the introduction of two terms, t_1 and t_2 :

$$\begin{cases} X_{S23} = X_{S1} + dd \\ Y_{S23} = Y_{S1} - \frac{l_{par}}{2} \\ Z_{S23} = Z_{S1} \end{cases}, \quad \begin{cases} t_1 = X_{S23}^2 + Y_{S23}^2 - 2 \cdot Y_{S23} \cdot Y_{q_3} + Y_{q_3}^2 \\ t_2 = X_{S23}^2 + Y_{S23}^2 - 2 \cdot Y_{S23} \cdot Y_{q_2} + Y_{q_2}^2 \end{cases} \quad (3)$$

Denoting with M the intersection point of the links connecting q_3 with the mobile platform and with N the point of intersection of the links connecting q_2 to the mobile platform, the following double solutions are obtained:

$$\begin{cases} X_M = \frac{X_{S23}}{2} \pm \left(\frac{Y_{S23} \mp Y_{q_3}}{2} \right) \cdot \sqrt{\frac{t_1 - 4 \cdot R^2}{t_1}} \\ Y_M = \frac{Y_{S23}}{2} + \frac{Y_{q_3}}{2} \mp \frac{X_{S23}}{2} \cdot \sqrt{\frac{t_1 - 4 \cdot R^2}{t_1}} \end{cases}, \quad \begin{cases} X_N = \frac{X_{S23}}{2} \pm \left(\frac{Y_{S23} \mp Y_{q_2}}{2} \right) \cdot \sqrt{\frac{t_2 - 4 \cdot R^2}{t_2}} \\ Y_N = \frac{Y_{S23}}{2} + \frac{Y_{q_2}}{2} \mp \frac{X_{S23}}{2} \cdot \sqrt{\frac{t_2 - 4 \cdot R^2}{t_2}} \end{cases} \quad (4)$$

To select the desired solution (as this set of double solutions leads to a total number of 4 working modes) the following conditions are imposed to select one solution: $Y_M = \min(Y_{M1,2})$, $Y_N = \max(Y_{N1,2})$. The equations for the active joints can be computed:

$$\begin{cases} q_1 = Z_{S1} + cc; \\ q_4 = Y_{S2} \\ q_5 = q_4 + \sqrt{lq_5^2 - (\text{abs}(X_{S2}) - lq_4 + ddd)^2} \end{cases}, \quad \begin{cases} q_2 = \pi - \arccos \left(\frac{Y_N - Y_{q_2}}{\sqrt{X_N^2 + (Y_N - Y_{q_2})^2}} \right) \\ q_3 = \pi - \arccos \left(\frac{Y_M - Y_{q_3}}{\sqrt{X_M^2 + (Y_M - Y_{q_3})^2}} \right) \end{cases} \quad (5)$$

The implicit functions are computed in order to solve the kinematic model for speeds and accelerations. Introducing the notations:

$$\begin{aligned} \text{Term1} &= \left(X_{E2}^2 - d \cdot \sin(\theta_{E2}) + dd \right)^2 + \left(Y_{E2}^2 - d \cdot \cos(\theta_{E2}) \cdot \sin(\psi_{E2}) - Yq_2 - \frac{l_{\text{par}}}{2} \right)^2, \\ \text{Term2} &= \left(X_{E2}^2 - d \cdot \sin(\theta_{E2}) + dd \right)^2 + \left(Y_{E2}^2 - d \cdot \cos(\theta_{E2}) \cdot \sin(\psi_{E2}) - Yq_3 - \frac{l_{\text{par}}}{2} \right)^2 \end{aligned} \quad (6)$$

It results that the expressions of the implicit functions can be written using eq. (1-6) as follows:

$$\begin{cases} f_1 = q_1 - Z_{E2} - d \cdot \cos(\psi_{E2}) \cdot \cos(\theta_{E2}) - cc \\ f_2 = \cos(\pi - q_2) - \frac{1}{2 \cdot R} \left(Y_{E2} + d \cos(\theta_{E2}) \sin(\psi_{E2}) - \frac{l_{\text{par}}}{2} - Yq_2 - (X_{E2} + d \cdot \sin(\theta_{E2}) + dd) \sqrt{\frac{4 \cdot R^2 - \text{Term1}}{\text{Term1}}} \right) \\ f_3 = \cos(\pi - q_3) - \frac{1}{2 \cdot R} \left(Y_{E2} + d \cos(\theta_{E2}) \sin(\psi_{E2}) - \frac{l_{\text{par}}}{2} - Yq_3 - (X_{E2} + d \cdot \sin(\theta_{E2}) + dd) \sqrt{\frac{4 \cdot R^2 - \text{Term2}}{\text{Term2}}} \right) \\ f_4 = q_4 - Y_{E2} - \left(d + \frac{l_{pp}}{\cos(\psi_{E2}) \cdot \cos(\theta_{E2})} \right) \cdot \sin(\psi_{E2}) \cdot \cos(\theta_{E2}) \\ f_5 = q_5 - q_4 - \sqrt{lq_5^2 - \left(ddd - lq_4 - \left(X_{E2} - \left(d + \frac{l_{pp}}{\cos(\psi_{E2}) \cdot \cos(\theta_{E2})} \right) \cdot \sin(\theta_{E2}) \right) \right)^2} \end{cases} \quad (7)$$

Using equation (7) the Jacobi matrices (**A** and **B** – calculated as the partial derivatives of the implicit function with respect to the end-effector coordinates, respectively the active joints) are determined enabling the solving of the kinematic model using the equations which characterize the speeds and accelerations.

$$\mathbf{A} \cdot \dot{\mathbf{X}} + \mathbf{B} \cdot \dot{\mathbf{Q}} = 0, \quad \mathbf{A} \cdot \ddot{\mathbf{X}} + \dot{\mathbf{A}} \cdot \dot{\mathbf{X}} + \dot{\mathbf{B}} \cdot \dot{\mathbf{Q}} + \mathbf{B} \cdot \ddot{\mathbf{Q}} = 0$$

$$\text{where } \dot{\mathbf{X}} = \begin{bmatrix} \dot{X}_{E2} & \dot{Y}_{E2} & \dot{Z}_{E2} & \dot{\theta}_{E2} & \dot{\psi}_{E2} \end{bmatrix}^T \text{ and } \dot{\mathbf{Q}} = \begin{bmatrix} \dot{q}_1 & \dot{q}_2 & \dot{q}_3 & \dot{q}_4 & \dot{q}_5 \end{bmatrix}^T, \text{ respectively} \quad (8)$$

$$\ddot{\mathbf{X}} = \begin{bmatrix} \ddot{X}_{E2} & \ddot{Y}_{E2} & \ddot{Z}_{E2} & \ddot{\theta}_{E2} & \ddot{\psi}_{E2} \end{bmatrix}^T \text{ and } \ddot{\mathbf{Q}} = \begin{bmatrix} \ddot{q}_1 & \ddot{q}_2 & \ddot{q}_3 & \ddot{q}_4 & \ddot{q}_5 \end{bmatrix}^T.$$

Case 2. The I-US probe is located inside the body. After the probe is inserted into the body it loses 2 DoFs because the motion becomes dependent on the insertion point or RCM. As a consequence, the input parameters change, becoming X_{E2} , Y_{E2} , Z_{E2} , X_B , Y_B , Z_B where B represents the RCM. Furthermore, after the insertion the probe distal head can perform the additional rotations presented in section 2.1, which introduces three additional parameters, namely the rotations around the three axes Z, X and Y, denoted with θ_s , ψ_s and φ_s . Introducing as a new parameter ud the length of the distal segment that bends it can be written that the coordinates of the bending point U are:

$$\begin{cases} X_U = X_{E2} - ud \cdot (\cos(\theta_s) \cdot \sin(\psi_s) - \sin(\theta_s) \cdot \cos(\psi_s) \cdot \sin(\varphi_s)) \\ Y_U = Y_{E2} - ud \cdot (\sin(\theta_s) \cdot \sin(\psi_s) + \cos(\theta_s) \cdot \cos(\psi_s) \cdot \sin(\varphi_s)) \\ Z_U = Z_{E2} - ud \cdot \cos(\varphi_s) \cdot \cos(\psi_s) \end{cases} \quad (9)$$

Knowing the coordinates of points U and B the orientation of the rigid segment of the I-US probe can be computed using trigonometric functions (arcsine – asin and arctangent 2 – atan2):

$$\theta_{E2} = \text{asin} \left(\frac{X_U - X_B}{\sqrt{(X_U - X_B)^2 + (Y_U - Y_B)^2 + (Z_U - Z_B)^2}} \right), \quad \psi_{E2} = \text{atan2}(Y_B - Y_U, Z_B - Z_U). \quad (10)$$

Using the coordinates of point U and keeping in mind that the distance between U and SI is d_{ud} the equations from 1 to 7 can be used to solve the kinematic model of the I-US guiding module. A set of numerical simulations illustrate the robot behaviour in a sequence presented in next Fig. 8.

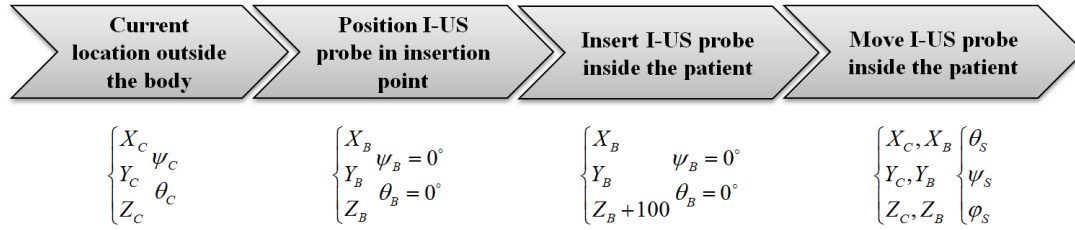


Fig. 8 – Movement sequence of the ProHep-LCT I-US probe guiding module.

4. NUMERICAL SIMULATIONS

A set of numerical simulations are presented to illustrate the robot behavior in several critical instances, using the following set of parameters (all values expressed in mm):

$$\begin{aligned} R = 315, l_{q4} = 325, l_{q5} = 400, Y_{q2} = 605, Y_{q3} = 225, d = 150, l_{pp} = 115, \\ cc = 85, l_{par} = 150, dd = 110, ddd = 125, ud = 70. \end{aligned} \quad (11)$$

Two numerical simulations are presented with respect to the medical procedure (Step 4 in table 1): (1) the motion of the I-US probe from an arbitrary point C in the point B (the insertion point inside the body) with the probe positioned vertically, (2) the motion of the I-US probe between two points inside the patient body (from point B to point C) including the bending of the distal head (defined by the three angles ψ_S, θ_S, ϕ_S which have *initial* and *final* values). The parameters for the two motions are defined below:

$$\begin{aligned} \begin{cases} X_C = -350 \text{ mm} \\ Y_C = 350 \text{ mm} \\ Z_C = 300 \text{ mm} \\ \psi_C = 30 \text{ deg} \\ \theta_C = 30 \text{ deg} \end{cases} \rightarrow \begin{cases} X_B = -450 \text{ mm} \\ Y_B = 320 \text{ mm} \\ Z_B = 250 \text{ mm} \\ \psi_B = 0 \text{ deg} \\ \theta_B = 0 \text{ deg} \end{cases} \begin{cases} X_C = -490 \text{ mm} \\ Y_C = 370 \text{ mm} \\ Z_C = 120 \text{ mm} \\ \psi_{Sinitial} = 0 \text{ deg} \\ \theta_{Sinitial} = 0 \text{ deg} \\ \phi_{Sinitial} = 0 \text{ deg} \end{cases} \begin{cases} X_B = -450 \text{ mm} \\ Y_B = 320 \text{ mm} \\ Z_B = 250 \text{ mm} \end{cases} \begin{cases} X_D = -530 \text{ mm} \\ Y_D = 420 \text{ mm} \\ Z_D = 80 \text{ mm} \\ \psi_{Sfinal} = -10 \text{ deg} \\ \theta_{Sfinal} = 15 \text{ deg} \\ \phi_{Sfinal} = 30 \text{ deg} \end{cases} \quad (12) \end{aligned}$$

Figure 9 illustrates the time history diagrams for displacements, speeds and accelerations of the active joints along with the variation of the I-US probe tip coordinates for the first motion which ends with the tip in the RCM (point B) with a specific orientation which enables the insertion inside the body. Figure 10 shows on the first column the displacement at the level of the 3 actuators that determine the orientation of the probe distal head from an initial set of bending angles (see section 2.1) followed, in the second column by the movement of the I-US probe from point C to point D while maintaining the previously defined point B which must remain fixed in space (based on the RCM concept) achieved with the actuators of the robotic module. The third column illustrates the variation of the position and orientation of the I-US probe tip during the two phases of the motion. The kinematic model has been validated in Siemens NX using the CAD model of the robot (Fig. 6) where the calculated motion parameters of the active joints were used as inputs for the motors showing a similar behavior of the structure.

5. CONCLUSIONS

A new approach in the targeted treatment of non-resectable HCC is presented, by integrating a robotic system that manipulates in the same time therapeutic needles inserting them in the targeted tumours and an I-

US probe used to monitor the needle placement in real-time. The advantages of this approach refer to the accuracy of the tumour targeting without complicated robot-patient calibration, as the I-US enables real-time monitoring and corrections of the needle position. A new modular parallel robotic system is proposed, based on a medical protocol, followed by a detailed analysis of the kinematics of the I-US probe guiding module with its particularities based on the probe location (outside/inside) the patient body. Numerical simulations of the I-US probe guiding module motions which follow the medical procedure validate the proposed solution. Future work will focus on singularities analysis and geometry optimizations for safety and workspace maximization, followed by the development of the first experimental model.

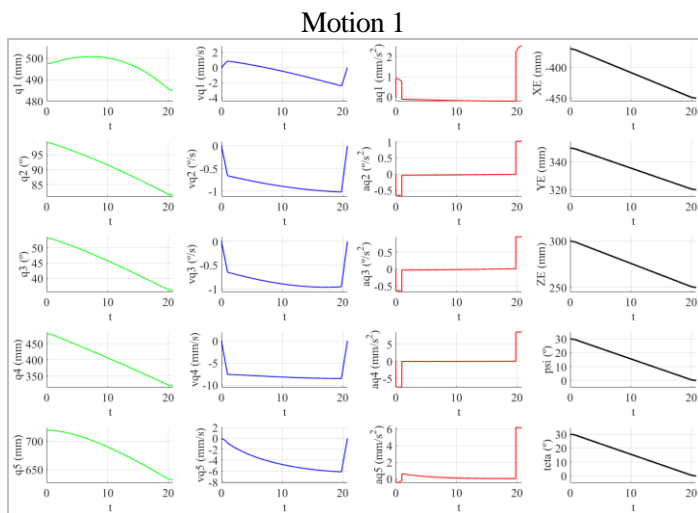


Fig. 9 – Time history diagram for active joints displacement speeds and accelerations for motion 1 along with the variation of the probe tip coordinates.

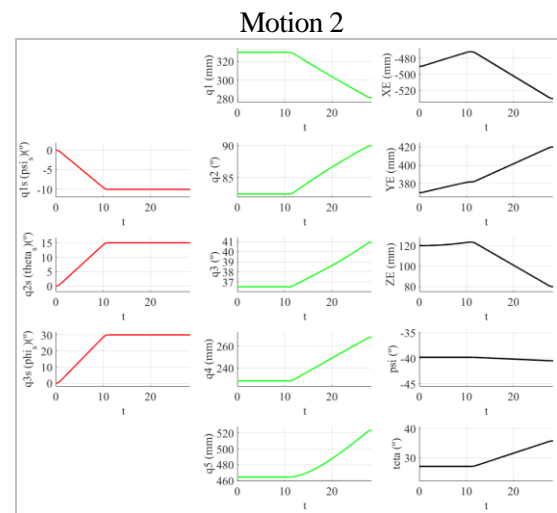


Fig. 10 – Time history diagrams for displacements during motion 2 (probe tip actuators – red, robot actuators – green, tip coordinates – black)

ACKNOWLEDGEMENTS

This work was supported by a grant of the Romanian Ministry of Research and Innovation, PCCCDI – UEFISCDI, project number PN-III-P1-1.2-PCCDI-2017-0221 / 59PCCDI/2018 (IMPROVE), within PNCDI III and by the GNaC 2018 ARUT grant “Innovative robotized instruments for treatment in surgical abdominal procedures”, Research Contract no. 3216/06.02.2019, with the financial support of the Technical University of Cluj-Napoca.

REFERENCES

1. A. WAGHRAY, A.R. MURALI, K.N. MENON, *Hepatocellular carcinoma: From diagnosis to treatment*, World J Hepatol, **7**, 8, pp. 1020-1029, 2015.
2. J.M. JIANG, N. OHRI, J. TANG, R. MOADE, J. CYNAMON, A. KAUBISCH, M. KINKHABWALA, M.K. GARG, C. GUHA, R. KABARRIT, *Centers with more therapeutic modalities are associated with improved outcomes for patients with hepatocellular carcinoma*, J. Gastrointest. Oncol., **10**, 3, pp. 546-553, 2019.
3. I. LURJE, Z. CZIGANY, J. BEDNARSCH, C. RODERBURG, P. ISFORT, U.P. NEUMANN, G. LURJE, *Treatment strategies for hepatocellular carcinoma – A multidisciplinary approach*, Int. J. Mol. Sci., **20**, 6, p. 1465, 2019.
4. K.P. LABADIE, S.K. SCHAUB, D. KHORSAND, G. JOHNSON, S. APISARNTHANARAX, J.O. PARK, *Multidisciplinary approach for multifocal, bilobar hepatocellular carcinoma: A case report and literature review*, World J. Hepatol., **11**, 1, pp. 119-126, 2019.
5. G. STRASSMAN, P. OLBERT, A. HEGELE, D. RICHTER, E. FOKAS, N. TIMMESFELD, R. HOFMANN, R. ENGENHART-CABILLIC, *Advantage of robotic needle placement on a prostate model in HDR brachytherapy*, Strahlenther Onkol., **187**, 6, pp. 367-272, 2011.
6. IMPROVE – <https://cester.utcluj.ro/improve/en/objectives.html>, last accessed July 9, 2019.
7. D. PISLA, I. BIRLESCU, C. VAIDA, P. TUCAN, A. PISLA, B. GHERMAN, N. CRISAN, N. PLITEA, *Algebraic modeling of kinematics and singularities for a prostate biopsy parallel robot*, Proc. Rom. Academy – A, **19**, 3, pp. 489-497, 2018.

8. D. PISLA, B. GALDAU, F. COVACIU, C. VAIDA, D. POPESCU, N. PLITEA, *Safety issues in the development of the experimental model for an innovative medical parallel robot used in brachytherapy*, Int. Journal of Production Research, **55**, 3, pp. 684-699, 2017.
9. C. VAIDA, I. BIRLESCU, N. PLITEA, N. CRISAN, D. PISLA, *Design of a needle insertion module for robotic assisted transperineal prostate biopsy*, in: *New Trends in Medical and Service Robots. Design, Analysis and Control*, pp. 1-15, 2016.
10. T.K. TANEV, *Minimally-invasive-surgery parallel robot with non-identical limbs*, IEEE/ASME 10th International Conference on Mechatronic and Embedded Systems and Applications (MESA), September 10-12, 2014
11. N. PLITEA, D. PISLA, C. VAIDA, B. GHERMAN, P. TUCAN, *PRoHep-LCT – Parallel robot for the minimally invasive treatment of liver cancer*, Patent pending, OSIM A01017/03.12.2018, 2018.
12. C. VAIDA, P. TUCAN, N. PLITEA, V. LAZAR, N. AL HAJJAR, D. PISLA, *Kinematic analysis of a new parallel robotic system for minimally invasive therapy of non-resectable hepatic tumors*, in: *Advances in Mechanism and Machine Science – Proceedings of the 15th IFToMM World Congress on Mechanism and Machine Science* ed. T. Uhl, **73**, pp. 719-728, 2019.

Received July 13, 2019